ACS APPLIED MATERIALS & INTERFACES

www.acsami.org

Research Article

Tough and Three-Dimensional-Printable Poly(2-methoxyethyl acrylate)−Silica Composite Elastomer with Antiplatelet Adhesion Property

Fumio Asai,* Takahiro Seki, Ayae Sugawara-Narutaki, Kazuhide Sato, Jérémy Odent, Olivier Coulembier, Jean-Marie Raquez, and Yukikazu Takeoka*

Cite This: *ACS Appl. Mater. Interfaces* 2020, 12, 46621−46628

Read Online

ACCESS | Metrics & More | Article Recommendations | Supporting Information

ABSTRACT: Poly(2-methoxyethyl acrylate) (PMEA) has attracted attention as a biocompatible polymer that is used as an antithrombotic coating agent for medical devices, such as during artificial heart and lung fabrication. However, PMEA is a viscous liquid polymer with low T_g, and its physical strength is poor even if a cross-linker is used, so it is difficult to make tough and freestanding objects from it. Here, we design and fabricate a biocompatible elastomer made of tough, self-supporting PMEA−silica composites. The toughness of the composite elastomer increases as a function of silica particle filling, and its stress at break is improved from 0.3 to 6.7 MPa. The fracture energy of the composite elastomer with 39.5 vol % silica particles is up to 15 times higher than that of the cross-linked PMEA with no silica particles and the material demonstrates stress−strain behavior that is similar to that of biological soft tissue, which exhibits nonlinear elasticity. In addition, the composite elastomer shows the potential to be an antithrombotic property, while the results of the platelet adhesion test of the composite elastomer show that the number of adhered platelets is not significantly affected by the silica addition. As the composite elastomer can be rapidly three-dimensional-printed into complex geometries with high-resolution features, it is expected to contribute to the development of medical devices from readily available materials.

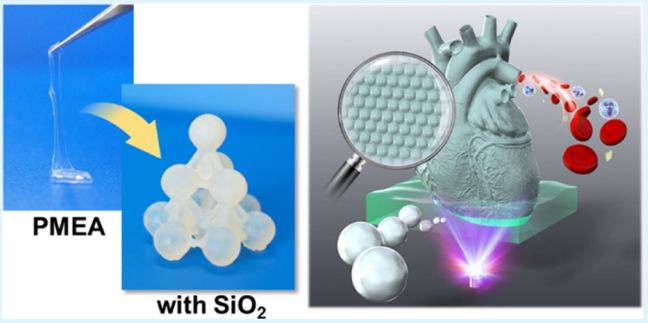

KEYWORDS: *composite elastomer, toughness, nonlinear elasticity, blood compatible, stereography*

1. INTRODUCTION

The biocompatibility of many polymer materials has been studied to date, and they have been put to practical use in medical devices and implant materials.[1] Blood compatibility is an important property that determines the application of polymers as biocompatible materials; in particular, suppressing the adhesion of platelets to a material surface is necessary to avoid thrombus formation.[2,3] As a method for suppressing the adhesion of platelets, various studies have been conducted on the control of the microstructure of the material surface.[4−7] Jiang et al. reported a polydimethylsiloxane film on the surface of which submicrometer ridges and nanoprotrusions were formed by utilizing self-assembly, soft lithography, and physical treatment processes.[8] Cao et al. presented materials with surfaces that contained microvalleys and were constructed by orienting long-chain branched poly(lactic acid) (b-PLA), exhibiting good mechanical properties and biocompatibility.[9] These studies attempted to implement blood compatibility by controlling the flow of fluid near the ridges or the microvalleys that replicated the inner surface structure of blood vessels; this approach appeared to make sense from the viewpoint of biomimicry. However, the process for forming these characteristic surface structures is complicated, and the macroscopic shape of the obtained material is limited. On the other hand, water-soluble polymers, such as poly(ethylene glycol) (PEG) and poly(methacryloyloxyethyl phosphorylcholine) (PMPC), are known to exhibit blood compatibility regardless of their surface morphology.[10−12] When these polymers contact blood, the local state of the water near the polymer interface affects the adhesion of proteins or cells, which is important for bioinertness.[13] Poly(2-methoxyethyl acrylate) (PMEA), which is also blood compatible, is a next-generation bioinert polymer with low water solubility.[14] Tanaka et al. classified the water existing near the surface of PMEA into three types [namely, nonfreezing water, intermediate water (IW), and free water] by

Received: June 23, 2020
Accepted: September 17, 2020
Published: September 17, 2020

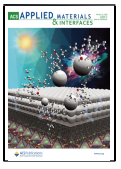

https://dx.doi.org/10.1021/acsami.0c11416
ACS Appl. Mater. Interfaces 2020, 12, 46621−46628

differential scanning calorimetry (DSC) measurements.[15] They revealed that the IW interacting with the methoxy side chain of PMEA plays an important role in blood compatibility (the IW is also present in PEG and PMPC).[16] To date, PMEA is expected to be widely used as a blood-compatible material, but it is mainly used only as a coating agent in practical use (e.g., for artificial heart/lung fabrication). PMEA has a low glass-transition temperature (T_g) and is a viscous liquid-like polymer, so its use is limited because it is not self-supporting. Suzuki et al. made a 1.2 mm thick film by casting a PMEA microsphere aqueous dispersion to obtain freestanding PMEA objects.[17] As PMEA microspheres could be obtained by emulsion polymerization in water, it was highlighted that this clean microsphere system offers new perspectives for application in medical devices. Tanaka et al. have shown that rubber-like hydrogen-bonded PMEA (H-PMEA) can be obtained by introducing multiple hydrogen bonding sites into the side chain of PMEA.[18] Films of various thicknesses could be fabricated from H-PMEA by pressing the material at 60 °C and 5 MPa, or by solvent casting. Fracture stress of the aforementioned PMEA films were respectively 0.58 and 1.1 MPa, which are low compared to general elastomers, and further toughening of PMEA films might be necessary for practical use. In addition, most of the reports are limited to film objects, and there are no examples showing complex geometries. Although there are these issues to be solved, the studies on recent attempts to prepare freestanding objects from PMEA imply the great need for smart processes for medical apparatus manufacturing. Recently, we reported a transparent composite elastomer composed of diethylene glycol monomethyl ether methacrylate ($PMEO_2MA$) and submicron spherical silica particles, which was inspired by the cornea, which is one of the extracellular matrices.[19] Spherical silica particles were fixed in colloidal crystals in the polymer matrix of this composite elastomer, and increasing the amount of silica significantly improved the strength and strain at break of the composite elastomer. Based on this result, we predicted that PMEA, which has a structure similar to $PMEO_2MA$, can be reinforced by the filling of silica particles to obtain a self-supporting composite elastomer that is blood compatible. Therefore, the purpose of this study is to prepare a composite elastomer mainly composed of PMEA and silica particles using additive manufacturing technology and investigate its mechanical properties and blood compatibility. Expectations for the practical application to medical devices include the ability to obtain desired three-dimensional (3D) objects safely and quickly without using sophisticated processing techniques or expensive equipment.[20] 3D printing of the composite elastomers herein represents a novel fabrication method to design blood-compatible soft materials into complex geometries with high-resolution features from readily available and safe substances for building medical devices. While degradable PEG-based systems are sought for medical purposes, some of us further provide a complete description of PEG polycondensate synthesis in solvent-free condition to obtain a mimetic and degradable PEG, respecting the workable definition of green chemistry, thus providing opportunities for future prospects based on the present study.[21] These results also show new possibilities for solving potential problems with blood-compatible materials.

2. EXPERIMENTAL SECTION

2.1. Materials. First, 2-methoxyethyl acrylate (MEA) 98% (1.01 g cm^{-3}, 130.14 g mol^{-1}, Tokyo Chemical Industry) was used as a monomer without purification. Diethylene glycol diacrylate (DEGDA) (1.12 g cm^{-3}, 214.22 g mol^{-1}, Tokyo Chemical Industry) was used as a cross-linking agent. Diphenyl(2,4,6-trimethylbenzoyl)-phosphine oxide (TPO) (348.37 g mol^{-1}, Sigma-Aldrich) was used as a photoinitiator. The ion-exchanged water was purified with a Millipore Milli-Q Labo system, and water with an electrical resistivity of 18.2 MΩ cm was used. A monodispersed fine silica powder with a particle size of 110 nm (2.221 g cm^{-3}, Silibol 110, Fuji Chemical) was used as the filler to prepare the composite elastomers. PET film with a thickness of 50 μm (EMBLET S-50, UNITIKA) was used as a control for the platelet adhesion test.

2.2. Analytical Techniques. Thermogravimetric analysis (TGA) was performed using a Shimadzu DTG-60 with an aluminum pan under nitrogen gas conditions. A TGA sample from 10 to 15 mg was placed in the pan, and an aluminum lid was placed on it. The empty pan with the lid was used as the reference. The sample was increased up to 500 °C from 20 °C (20 °C min^{-1}) and then held for 1 h.

The density measurements were performed with a Micromeritics Instrument Corporation AccuPyc 1330 pycnometer (Helium gas, 25 °C). The gel permeation chromatography (GPC) measurement was performed with a Shodex DS-4/UV-41/RI-101 connected with three GPC columns (Shodex KF-403, KF-404, and KF-405). THF was used as an eluent at a flow rate of 1.0 mL min^{-1}. The calibration of the molecular weight was achieved by using polystyrene standards (TSK standard polystyrene, Tosoh).

2.3. 3D Printing. A suspension of MEA and DEGDA (200:1 molar ratio) containing 27 vol % of the silica particles was sonicated (1500 J cm^{-3}) using an ultrasonic homogenizer (UP200St, Hielscher Ultrasonics). Subsequently, this suspension to which TPO (1.0 mol %) was added was used as the monomer suspension for 3D printing. By using an MSLA 3D printer (iSUN3D, Shenzhen Esun Industrial), 3D printing of the composite elastomer was performed (405 nm, exposure time 7 s, 100 μm/layer).

2.4. Cross-Section Observations. To prepare cross-section samples for observation, the composite elastomers underwent an ion polishing treatment using a Gatan model 693 Precision Ion Polishing System (−160 °C, 4 keV, 6 h). The cross-section samples were sputter-coated with platinum and observed by using field emission scanning electron microscopy (FE-SEM) (SU8020, Hitachi High-Technologies).

2.5. Mechanical Properties. The uniaxial tensile tests were carried out using a Shimadzu EZ-Test (50 mm min^{-1}). The ISO37-4 dumbbell-type test pieces used for the test were prepared by punching the 1 mm thick composite elastomer sheet using a Super Dumbbell Cutter (SDMP-1000-D, Dumbbell).

2.6. Human Platelet Adhesion Test. Sodium citrate (3.2% aqueous solution) was added to human whole blood for use in this test. The platelet-rich plasma (PRP) was collected by centrifuging (200 g, 5 min) the blood suspension with a high-speed refrigerated centrifuge, and the platelet-poor plasma (PPP) was collected after further centrifugation (1500*g*, 10 min). The number of platelets in the PRP and PPP was counted with an optical microscope, and the platelet suspension was prepared by adding PPP to the PRP so that the platelet density was 1.75×10^7 cells mL^{-1}. The PET film and composite elastomer sheets were cut into a square of 8 mm, and the platelet suspension (200 μL) was placed on each sheet and incubated (37 °C, 1 h). Each sheet was washed twice with phosphate buffered saline (PBS) and fixed with 1.0% glutaraldehyde in PBS (37 °C, 2 h). These sheets were washed sequentially with PBS, a solution of PBS/water = 1:1 and water. After drying, the sheets were sputter-coated with osmium tetroxide, and the number of platelets adhering to the surface was counted using FE-SEM (JSM-7500FA, JEOL). The platelets are classified into three types according to the number of pseudopodia: 0; type 1, 1−2; type 2, and more than 2; type 3. The test was performed three times, and the average numbers of platelets

https://dx.doi.org/10.1021/acsami.0c11416
ACS Appl. Mater. Interfaces 2020, 12, 46621−46628

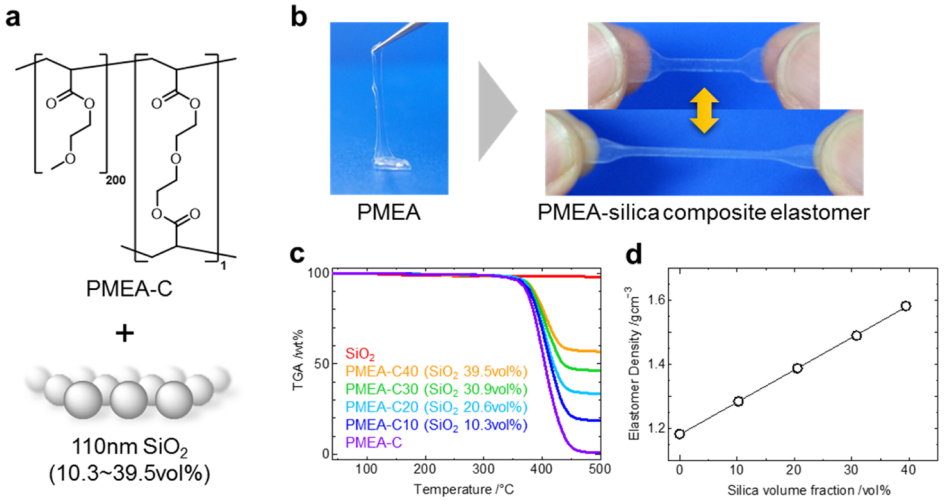

Figure 1. Silica particles fixed in the composite elastomer. (a) Schematic of the material composition. (b) Image showing the extensibility of the dumbbell-shaped composite elastomer. (c) TGA chart of silica particles and each composite elastomer. PMEA-C, PMEA-C10, PMEA-C20, PMEA-C30, and PMEA-C40 represent composite elastomers containing 0, 10.3, 20.6, 30.9, and 39.5 vol % silica particles, respectively. (d) Dependence of the density of the composite elastomers on the amount of silica particles.

that adhered to the surface in each of the five fields of view were calculated.

The ethical board of Nagoya University, Clinical Research Committee, approved the use of human biological samples (healthy human whole blood) (approval #2017-0534).

3. RESULTS AND DISCUSSION

3.1. Preparation of the Composite Elastomer. In this study, various amounts of powdered silica particles were mixed in solutions that contained a mixture of MEA and DEGDA, a cross-linking agent, at a ratio of 200:1 (Figure 1a). Suspensions containing 0, 9, 18, 27, and 36 vol % silica particles with an average diameter of 110 nm were prepared. The suspension was sonicated (1500 J cm^{-3}) using an ultrasonic homogenizer, and TPO (0.1 mol %) was added. Then, the suspension was poured into a mold with a 1 mm thick silicon rubber spacer sandwiched between two glass plates and irradiated with ultraviolet light for photopolymerization (10 mW cm^{-2}, 120 s) (Figure S1). The obtained PMEA−silica composite elastomers were colorless, transparent, and elastic (Figure 1b). These were named PMEA-C, PMEA-C10, PMEA-C20, PMEA-C30, and PMEA-C40 based on the silica particle content. The TGA results of the composite elastomers are shown in Figure 1c. As the weight loss of the PMEA and each composite elastomer started at approximately 350 °C, the silica filling had no effect on the thermal stability of the polymer. The volume fraction (ϕ) of the silica particles in the composite elastomer was calculated by eq 1

$$\phi = \frac{(\mathrm{TG} - 0.4) \times \mathrm{ED}}{97.7 \times 2.221} \times 100 \quad (1)$$

The residue of the composite elastomer (TG: 17.8, 32.6, 45.4, and 54.6 wt %), the residue of PMEA (0.4 wt %), the residue of the silica particles (97.7 wt %), the density of silica particles (2.221 g cm^{-3}), and the density of the elastomers (ED: 1.183, 1.284, 1.387, 1.489, and 1.582 g cm^{-3}) were used. The calculated values of ϕ for PMEA-C10, PMEA-C20, PMEA-C30, and PMEA-C40 were 10.3, 20.6, 30.9, and 39.5 vol %, respectively (Table S1). The density of the composite elastomers as measured by a gas pycnometer increased linearly with ϕ, indicating that the matrix polymers did not undergo a significant densification upon increasing the organic−inorganic interface (Figure 1d). The volume shrinkage of the PMEA and the matrix polymer in the composite elastomer determined from these results was approximately 14%.

3.2. 3D Printing of the Composite Elastomer. We carried out 3D printing of the composite elastomer by using commercial stereolithography (SLA) technology. In recent years, SLA 3D printers have become increasingly popular, which are small and relatively inexpensive for general consumers. The potential of the composite elastomer for practical use is supported by the general use of this apparatus for fabricating objects with a variety of complex 3D geometries. Here, the suspension of MEA containing silica particles (27 vol %) was used to perform SLA 3D printing using an MSLA 3D printer (100 μm/layer). As shown in Figure 2a, it was possible

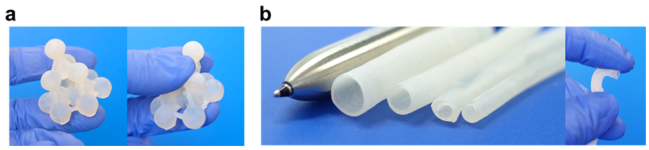

Figure 2. 3D printing of the composite elastomer. (a) Image showing the flexibility of the 3D printed object. (b) Image showing 3D printed tubes with different diameters, which are 8, 6, 5, and 4 mm from the one next to the ballpoint pen.

to form a flexible solid object composed of a sphere and a tetrahedron with high precision. In additive manufacturing, each layer has a submillimeter difference, while the resolution is approximately 50 μm. Therefore, the surface is not smooth, and the object has a whitish appearance. To show the possibility of application to artificial blood vessels, tubes with diameters of less than 8 mm were fabricated (Figure 2b). Currently, popular artificial blood vessels are mainly made of PET or fluoropolymers, but they are limited to larger diameter products because occlusion by thrombus is inevitable at diameters less than 6 mm. If the composite elastomer can be used to produce thinner artificial blood vessels than the previous elastomer, then it should have useful medical applications.

https://dx.doi.org/10.1021/acsami.0c11416
ACS Appl. Mater. Interfaces 2020, 12, 46621−46628

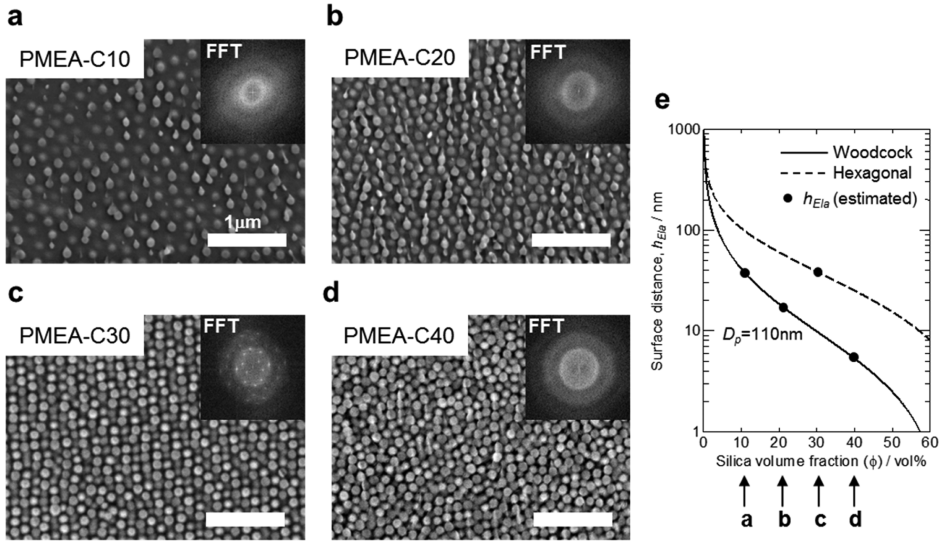

Figure 3. Array of the silica particle in composite elastomers. (a–d) Cross-sectional SEM images of the composite elastomers with different amounts of silica particles. The inset shows a FFT image of the SEM image. (e) Dependence of the volume fraction of silica particles on the expected distance between the particle surfaces. The arrows at the bottom of the graph correspond to the silica volume fractions in the composite elastomers observed by SEM.

3.3. Array of Silica Particles in Composite Elastomers.

To confirm the array of silica particles fixed in the composite elastomers, the cross sections of each composite elastomer were observed by scanning electron microscopy (SEM). The SEM images of the PMEA-C10 and PMEA-C20 show a halo pattern in the fast Fourier transform (FFT) image; hence, the particles in these samples had an isotropic alignment with short-range order (Figure 3a,b). In the section of PMEA-C30, multiple peaks can be observed in the FFT image, and it can be seen that the silica particles were aligned as in a colloidal crystal (Figure 3c). Furthermore, in PMEA-C40, where the volume fraction of silica increased to 39.5 vol %, the halo pattern was observed again in the FFT image, and the particles became isotropically oriented again (Figure 3d). As the filler amount increased, the particle arrays in the composite elastomers changed sequentially to having short-range order and forming colloidal crystals and colloidal amorphous structures. Megen et al. observed suspensions of polymethylmethacrylate (PMMA) particles (305 nm) modified with long alkyl chains and found that the crystallization of particles by local freezing began at an effective volume fraction of 49.4 vol % of the hard spheres, and the crystalline state became thermodynamically stable above 54.5 vol %.[22] However, if the volume fraction exceeded 57 vol %, crystallization became difficult because of suppression of particle diffusion, and a metastable amorphous phase was formed. Blaaderen et al., upon direct observation of the Brownian time in colloidal suspensions of PMMA–silica core–shell particles (450 nm), reported that particle diffusion did not proceed at all times above 57 vol %, and the pair correlation function showed the presence of crystalline arrays at 60 vol %.[23] In the Woodcock equation for a system with fine dispersed particles, the average particle surface distance h_{Ela} is obtained by a function of the particle diameter and particle concentration, as given by eq 2[24]

$$h_{Ela} = D_p\left\{\sqrt{\left(\frac{1}{3\pi\phi} + \frac{5}{6}\right)} - 1\right\} \quad (2)$$

where ϕ is the particle volume fraction and D_p is the particle diameter. The h_{Ela} when the particle array is hexagonally close packed, which is referred to as a colloidal crystal, can be calculated from eq 3[25]

$$h_{Ela} = D_p\left\{\left(\frac{\pi}{3\sqrt{2}\phi}\right)^{1/3} - 1\right\} \quad (3)$$

In Figure 3e, the relationship between the silica volume fraction and h_{Ela} is shown, and the curves are described according to eqs 2 and 3. Under the condition where the amorphous phase forms, the h_{Ela} calculated from the result provided by Megen (305 nm and 57 vol %) was 3.0 nm according to eq 2. The h_{Ela} for PMEA-C40 with the amorphous phase was 5.5 nm, which is in the same range as Megen's results. The particle morphology in the 30.9 vol % composite elastomer (PMEA-C30) was that of a colloidal crystal, and the h_{Ela} of a colloidal crystal derived from eq 3 was 37.2 nm. Similarly, the h_{Ela} values calculated with reference to the conditions reported by Megen and Blaaderen where crystallization was confirmed were respectively 32.8 nm (305 nm and 54.5 vol %) and 32.7 nm (450 nm and 60 vol %), which are close to the value of PMEA-C30. From the above results, sequential changes of the particle arrays in composite elastomers by filler amounts, which were seen in SEM images, correspond to the particle morphology in the reported colloidal suspension systems. It is considered that the particle arrangement changed from the crystalline state to the amorphous state because of the suppression of particle diffusion; this occurred because the distance between the surfaces of the silica particles in the MEA decreased. These facts are also supported by the fact that the MEA suspension containing 45 vol % silica particles became viscous and could not flow after sonication.

3.4. Toughening of the Composite Elastomers.

The composite elastomers were toughened as a result of their increased strength and extensibility because of interfacial interactions between the PMEA and the silica particles. Figure 4a shows the stress–strain curves obtained from uniaxial

https://dx.doi.org/10.1021/acsami.0c11416
ACS Appl. Mater. Interfaces 2020, 12, 46621–46628

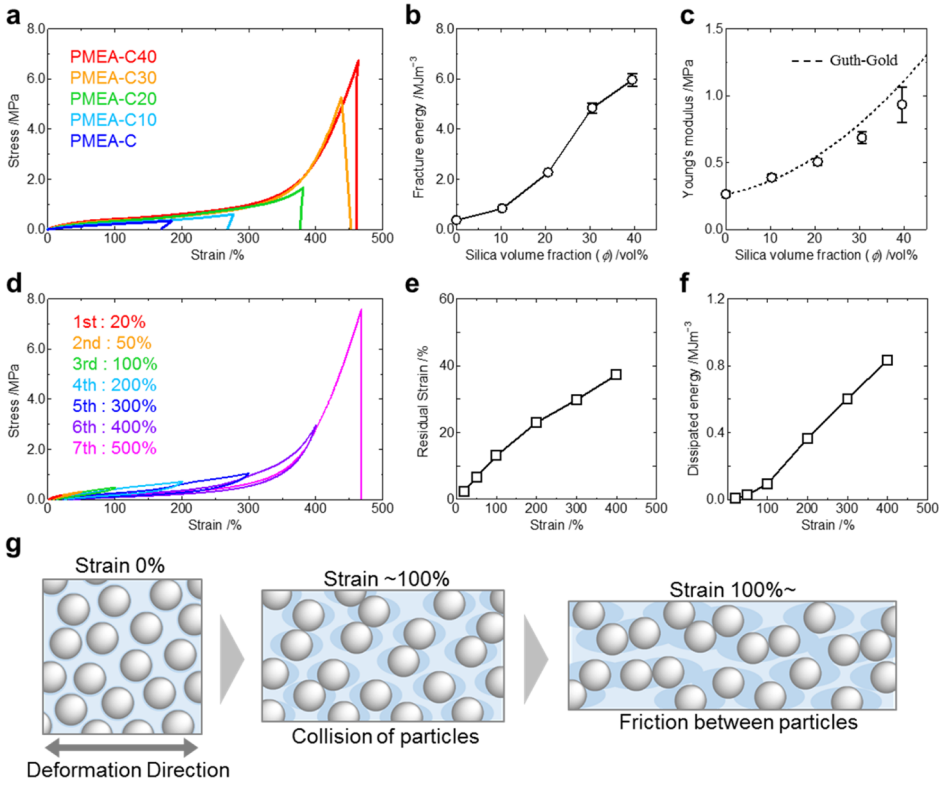

Figure 4. Mechanical properties of the composite elastomer. (a) Stress−strain curves of composite elastomers in which various amounts of 110 nm silica particles are dispersed. (b) Fracture energy at different silica particle amounts. (c) Young's modulus at different silica particle amounts. The dashed line shows the correlation between Young's modulus and filler amounts expected from the Guth−Gold relation. (d) Stress−strain curve of PMEA-C40 from the hysteresis measurement. (e) Dependence of the residual strain on the predetermined strain. (f) Dissipated energy at each cycle in the hysteresis measurement. (g) A conceptual diagram for predicting the particle morphology under the deformation of the composite elastomer.

stretching of the composite elastomers prepared with various silica particle amounts. The Young's modulus and the fracture energy of PMEA-C containing no silica particles were respectively 0.26 MPa and 0.4 MJ m^{-3}, which is consistent with a soft and brittle material. Surprisingly, both the stress and the strain at break were found to be improved significantly with increasing the amount of silica particles. When an elastomer, such as rubber, contains a filler, the stress is usually increased, but the extensibility is generally almost unchanged or decreased. Herein, the fracture energy of PMEA-C40 was up to 15 times higher than that of PMEA-C (Figure 4b). In addition, increasing the amount of silica particles resulted in little change of the stress−strain curve shape between 0 and 300% strain, showing excellent flexibility even when the composite elastomer was reinforced. Notably, the absorbed water content of PMEA-C40 was 2.2 wt % after water equilibrium, and there was only a slight change in the stress−strain curve (Figure S4). Therefore, the constant contact of the composite elastomer with blood would not significantly reduce the toughness of the composite elastomer. The mechanism of reinforcement caused by the dispersion of a filler in an elastomer is explained qualitatively by the Guth−Gold relation,[26] which extends Einstein's viscosity theory. Assuming that the Young's modulus when no filler is incorporated is E_0, the volume fraction of the filler is ϕ, and the Young's modulus of the composite elastomer containing filler is E, the Guth−Gold relation is expressed by eq 4

$$E = (1 + 2.5\phi + 14.1\phi^2)E_0 \quad (4)$$

The correlation between the Young's modulus of the composite elastomers and the volume fraction of the silica particle is similar to the curve obtained from the Guth−Gold relation (Figure 4c). It is well known that the Young's modulus of elastomers that contain fillers becomes higher than that of the Guth−Gold relation as the filler amount increases.[27] Einstein's viscosity theory, which is the basis of the Guth−Gold relation, assumes the behavior of a monodispersed system without aggregation in a dispersed medium, whereas in an actual elastomer that contains a filler, the fillers form a network of aggregates.[28] The Young's modulus of the composite elastomer is applicable to the Guth−Gold relationship because there was almost no network of aggregated silica particles. In other words, the reason the composite elastomer was flexible at initial strains but able to withstand a high stress at high strains is that the silica particles were dispersed and there were no aggregate networks. Then, we discuss the possible reason why the toughness of the composite elastomer was significantly enhanced. The several results of MD simulations have mentioned that the entanglement of polymer chains is reduced in nanoparticle-reinforced polymers.[29−31] Thus, the extendibility of the composite elastomer would have increased because the entanglement, which is the point of fracture, would have decreased with increasing amounts of silica particles. In addition, the reduction of entanglements would have resulted in an increase in the number of fully extended chains under large deformations, resulting in a nonlinear elasticity. A nonlinearity of the stress−strain relation in which the stress rises significantly at large elongations is

https://dx.doi.org/10.1021/acsami.0c11416
ACS Appl. Mater. Interfaces 2020, 12, 46621−46628

observed for soft biological tissues.[32,33] This mechanical behavior that makes soft biological tissues less deformable as they elongate is known to help prevent catastrophe (such as a sudden large rupture). Although there are few artificial materials that exhibit such behavior, the composite elastomers in this study have the exact properties of soft biological tissues.

Next, the results of the hysteresis test of PMEA-C40 are shown in Figure 4d. In this test, the composite elastomer was deformed to a predetermined strain and then recovered until the stress reached zero. A series of cycles at each predetermined strain (20, 50, 100, 200, 300, 400 and 500% at 50 mm min^{-1}) were performed sequentially, and the results were measured up to when the specimens broke. There was no wait between the cycles. The stress−strain curve for each cycle shows a hysteresis loss, which is known as the Mullins effect.[34] The residual strain increased linearly with increasing strain and was approximately 10% of each prescribed strain (Figure 4e). From the previous discussion of the Young's modulus and SEM images, it was predicted that there was almost no aggregate network comprising the silica particles in the composite elastomer. Hence, the presence of the hysteresis loss can be understood as the result of the dissipation of the energy of the interaction between the silica particles and the matrix polymer during deformation. The dissipated energy in each cycle increased significantly from 100% strain (Figure 4f). This rise in dissipated energy is expected to be caused by a change in the interaction of the polymer−silica interface and the energy dissipation due to the collision of silica particles and the friction between the particles under a large strain (Figure 4g). In this composite elastomer, the organic−inorganic interface interaction and the interparticle interaction are at least two reinforcing effects that may be responsible for the toughening under deformation.

3.5. Platelet Adhesion Test with Human Blood. The platelet adhesion test is the most direct and popular evaluation method for confirming the blood compatibility of polymeric materials. Here, the platelet adhesion onto the surface of the composite elastomer was found to be suppressed, and the number of platelets that adhered to the surface was not significantly increased with increasing amounts of silica particles, although the surface was uneven. The results of the platelet adhesion test using human whole blood and the composite elastomer are shown in Figure 5a. To confirm if the presence of cross-linkers affects the number of adhered platelets, the polymer of MEA with no cross-linker (PMEA) (M_n = 200 k and M_w/M_n = 2.1) was prepared with the same photopolymerization procedure as that for the composite elastomer. The solution of the polymer (20 wt % in THF) was applied on a PET film using a doctor blade, and the dried film was used as the PMEA sample. The blood compatibility of PMEA-C is slightly lower than that of PMEA but is significantly superior to that of PET. Tanaka reported that H-PMEA is slightly less blood compatible than PMEA.[18] The PMEA led to a reduction in the IW that is considered to suppress platelet adhesion, and cross-linking sites reduced both the molecular mobility and the free volume of the polymer chains. The number of platelets that adhered to each composite elastomer (PMEA-C10, PMEA-C20, and PMEA-C40) was almost comparable to that of PMEA-C. Multiple pseudopod-extended platelets were present in the PET but were absent in each composite elastomer (Figure 5b−e). Remarkably, the increase in the amount of silica particles had little or no significant effect on the number of platelets. The

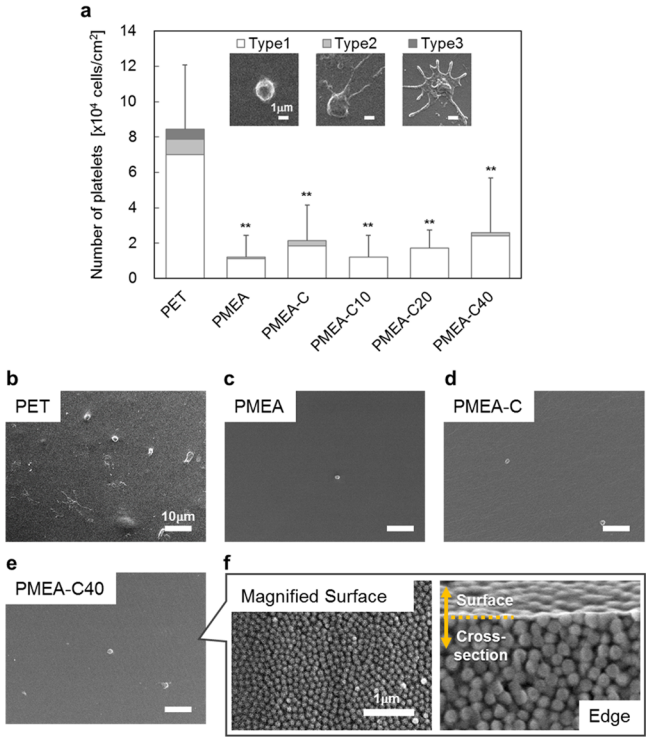

Figure 5. Blood compatibility of the composite elastomer. (a) Platelet adhesion test with human blood of the composite elastomer. A PET film was used as a control (the data represent mean value ± s.d., $^{**}P < 0.01$ vs PET). The number of platelets was classified into the following three types (shown in the inset) according to the activated state: (Type 1) spherical, (Type 2) hemispherical with several pseudopods, and (Type 3) spread-shaped with several pseudopods. (b−e) SEM images of platelets that adhered to the PET, PMEA, PMEA-C, and PMCA-C40 surfaces. (f) High-magnification SEM image of PMEA-C40, which focused on the surface and the edge of the cross section.

SEM image of the composite elastomer surface shows the presence of unevenness due to the shape of the silica particles (Figure 5f). The presence of a thin PMEA layer on silica particles can be confirmed from the edge image in Figure 5f. The presence of a thin PMEA layer on the top surface may have inhibited the adhesion of platelets even at high silica content.

4. CONCLUSIONS

In summary, we demonstrated a PMEA−silica composite elastomer with nonlinear elasticity and blood compatibility that could be rapidly 3D-printed by using commercial SLA technology. The toughness of the composite elastomer improved with increasing silica particle amount, and the fracture energy of the 39.5 vol % system was 15 times higher than that of the system with no silica particles. The correlation between the Young's modulus of the composite elastomers and the Guth−Gold relation suggests that the silica particles were fixed in the polymer matrix with no network of aggregates. The mechanical behavior of the composite elastomers was similar to that of soft biological tissue, demonstrating its ability to prevent catastrophes. It has been reported that bottlebrush polymers provide materials with mechanical properties similar to those of biological tissue structures[35,36] However, a multistep synthesis and purification step cannot be avoided to obtain the desired polymer. On the other hand, it is worth

https://dx.doi.org/10.1021/acsami.0c11416
ACS Appl. Mater. Interfaces 2020, 12, 46621−46628

noting that the composite elastomer we developed herein can be prepared in a short time under mild conditions and from a safe material that is readily available. The platelet adhesion test showed that there was no significant increase in the number of platelets after filling PMEA with silica particles, and the composite elastomer was superior to PET in terms of the blood compatibility. We printed the composite elastomer using an MSLA 3D printer, showing its high potential for practical applications. Applying the composite elastomer to blood-compatible materials will require detailed biocompatibility assessments, the selection of safe initiators, and a reduction in residual compounds. We expect that the composite elastomer in this study could contribute to new medical devices and the advancement of medicine.

■ ASSOCIATED CONTENT

Supporting Information

The Supporting Information is available free of charge at https://pubs.acs.org/doi/10.1021/acsami.0c11416.

Preparation of the composite elastomer; TGA; density measurements; cross-sectional SEM image; DSC measurements; results of uniaxial tensile test; mechanical property of the composite elastomer after water equilibrium; and SEM images of the human platelet adhesion test (PDF)

■ AUTHOR INFORMATION

Corresponding Authors

Fumio Asai − *Department of Molecular & Macromolecular Chemistry, Nagoya University, Nagoya 464-8603, Japan; Research & Development Center, Unitika Ltd., Uji-Shi, Kyoto 611-0021, Japan;* orcid.org/0000-0002-2690-1187; Email: asai.fumio@c.mbox.nagoya-u.ac.jp

Yukikazu Takeoka − *Department of Molecular & Macromolecular Chemistry, Nagoya University, Nagoya 464-8603, Japan*; Email: ytakeoka@chembio.nagoya-u.ac.jp

Authors

Takahiro Seki − *Department of Molecular & Macromolecular Chemistry, Nagoya University, Nagoya 464-8603, Japan*

Ayae Sugawara-Narutaki − *Department of Energy Engineering, Nagoya University, Nagoya 464-8603, Japan*

Kazuhide Sato − *Nagoya University Institute for Advanced Research, Nagoya 464-8601, Japan; Respiratory Medicine, Nagoya University Graduate School of Medicine, Nagoya 466-8550, Japan*

Jérémy Odent − *Laboratory of Polymeric and Composite Materials, Center of Innovation and Research in Materials and Polymers, University of Mons, 7000 Mons, Belgium;* orcid.org/0000-0002-3038-846X

Olivier Coulembier − *Laboratory of Polymeric and Composite Materials, Center of Innovation and Research in Materials and Polymers, University of Mons, 7000 Mons, Belgium;* orcid.org/0000-0001-5753-7851

Jean-Marie Raquez − *Laboratory of Polymeric and Composite Materials, Center of Innovation and Research in Materials and Polymers, University of Mons, 7000 Mons, Belgium;* orcid.org/0000-0003-1940-7129

Complete contact information is available at: https://pubs.acs.org/10.1021/acsami.0c11416

Notes

The authors declare no competing financial interest.

■ ACKNOWLEDGMENTS

This work was supported by UNITIKA LTD. J.-M.R. and O.C. are research associates at F.R.S.-FNRS (Belgium). J.O. gratefully acknowledges the Wallonie-Bruxelles International (WBI) for its mobility grant.

■ REFERENCES

(1) Jagur-Grodzinski, J. Polymers for Tissue Engineering, Medical Devices, and Regenerative Medicine. Concise General Review of Recent Studies. *Polym. Adv. Technol.* **2006**, *17*, 395−418.

(2) Liu, X.; Yuan, L.; Li, D.; Tang, Z.; Wang, Y.; Chen, G.; Chen, H.; Brash, J. L. Blood Compatible Materials: State of the Art. *J. Mater. Chem. B* **2014**, *2*, 5718−5738.

(3) Wei, Q.; Becherer, T.; Angioletti-Uberti, S.; Dzubiella, J.; Wischke, C.; Neffe, A. T.; Lendlein, A.; Ballauff, M.; Haag, R. Protein Interactions with Polymer Coatings and Biomaterials. *Angew. Chem., Int. Ed.* **2014**, *53*, 8004−8031.

(4) Koh, L. B.; Rodriguez, I.; Venkatraman, S. S. The Effect of Topography of Polymer Surfaces on Platelet Adhesion. *Biomaterials* **2010**, *31*, 1533−1545.

(5) Sun, T.; Tan, H.; Han, D.; Fu, Q.; Jiang, L. No Platelet Can Adhere—Largely Improved Blood Compatibility on Nanostructured Superhydrophobic Surfaces. *Small* **2005**, *1*, 959−963.

(6) Chen, L.; Liu, M.; Bai, H.; Chen, P.; Xia, F.; Han, D.; Jiang, L. Antiplatelet and Thermally Responsive Poly(N-Isopropylacrylamide) Surface with Nanoscale Topography. *J. Am. Chem. Soc.* **2009**, *131*, 10467−10472.

(7) Chen, L.; Han, D.; Jiang, L. On Improving Blood Compatibility: From Bioinspired to Synthetic Design and Fabrication of Biointerfacial Topography at Micro/Nano Scales. *Colloids Surf., B* **2011**, *85*, 2−7.

(8) Fan, H.; Chen, P.; Qi, R.; Zhai, J.; Wang, J.; Chen, L.; Chen, L.; Sun, Q.; Song, Y.; Han, D.; Jiang, L. Greatly Improved Blood Compatibility by Microscopic Multiscale Design of Surface Architectures. *Small* **2009**, *5*, 2144−2148.

(9) Li, J.; Chen, Q.; Zhang, Q.; Fan, T.; Gong, L.; Ye, W.; Fan, Z.; Cao, L. Improving Mechanical Properties and Biocompatibilities by Highly Oriented Long Chain Branching Poly(Lactic Acid) with Bionic Surface Structures. *ACS Appl. Mater. Interfaces* **2020**, *12*, 14365−14375.

(10) Banerjee, I.; Pangule, R. C.; Kane, R. S. Antifouling Coatings: Recent Developments in the Design of Surfaces That Prevent Fouling by Proteins, Bacteria, and Marine Organisms. *Adv. Mater.* **2011**, *23*, 690−718.

(11) Xia, Y.; Adibnia, V.; Shan, C.; Huang, R.; Qi, W.; He, Z.; Xie, G.; Olszewski, M.; De Crescenzo, G.; Matyjaszewski, K.; Banquy, X.; Su, R. Synergy between Zwitterionic Polymers and Hyaluronic Acid Enhances Antifouling Performance. *Langmuir* **2019**, *35*, 15535−15542.

(12) Seo, J.-H.; Matsuno, R.; Lee, Y.; Konno, T.; Takai, M.; Ishihara, K. Effect of Hydrophilic Polymer Conjugation on Heat-Induced Conformational Changes in a Protein. *Acta Biomater.* **2011**, *7*, 1477−1484.

(13) Chen, S.; Li, L.; Zhao, C.; Zheng, J. Surface Hydration: Principles and Applications toward Low-Fouling/Nonfouling Biomaterials. *Polymer* **2010**, *51*, 5283−5293.

(14) Tanaka, M.; Motomura, T.; Kawada, M.; Anzai, T.; Kasori, Y.; Shiroya, T.; Shimura, K.; Onishi, M.; Mochizuki, A. Blood Compatible Aspects of Poly(2-Methoxyethylacrylate) (PMEA)—Relationship between Protein Adsorption and Platelet Adhesion on PMEA Surface. *Biomaterials* **2000**, *21*, 1471−1481.

(15) Tanaka, M.; Hayashi, T.; Morita, S. The Roles of Water Molecules at the Biointerface of Medical Polymers. *Polym. J.* **2013**, *45*, 701−710.

(16) Morita, S.; Tanaka, M.; Ozaki, Y. Time-Resolved In Situ ATR-IR Observations of the Process of Sorption of Water into a Poly(2-Methoxyethyl Acrylate) Film. *Langmuir* **2007**, *23*, 3750−3761.
(17) Kureha, T.; Hiroshige, S.; Matsui, S.; Suzuki, D. Water-Immiscible Bioinert Coatings and Film Formation from Aqueous Dispersions of Poly(2-Methoxyethyl Acrylate) Microspheres. *Colloids Surf., B* **2017**, *155*, 166−172.
(18) Jankova, K.; Javakhishvili, I.; Kobayashi, S.; Koguchi, R.; Murakami, D.; Sonoda, T.; Tanaka, M. Hydration States and Blood Compatibility of Hydrogen-Bonded Supramolecular Poly(2-Methoxyethyl Acrylate). *ACS Appl. Bio Mater.* **2019**, *2*, 4154−4161.
(19) Watanabe, K.; Miwa, E.; Asai, F.; Seki, T.; Urayama, K.; Nakatani, T.; Fujinami, S.; Hoshino, T.; Takata, M.; Liu, C.; Mayumi, K.; Ito, K.; Takeoka, Y. Highly Transparent and Tough Filler Composite Elastomer Inspired by the Cornea. *ACS Mater. Lett.* **2020**, *2*, 325−330.
(20) Odent, J.; Wallin, T. J.; Pan, W.; Kruemplestaedter, K.; Shepherd, R. F.; Giannelis, E. P. Highly Elastic, Transparent, and Conductive 3D-Printed Ionic Composite Hydrogels. *Adv. Funct. Mater.* **2017**, *27*, 1701807.
(21) Moins, S.; Loyer, P.; Odent, J.; Coulembier, O. Preparation of a Mimetic and Degradable Poly(Ethylene Glycol) by a Non-Eutectic Mixture of Organocatalysts (NEMO): Via a One-Pot Two-Step Process. *RSC Adv.* **2019**, *9*, 40013−40016.
(22) Pusey, P. N.; Van Megen, W. Phase Behaviour of Concentrated Suspensions of Nearly Hard Colloidal Spheres. *Nature* **1986**, *320*, 340−342.
(23) Kegel, W. K.; van Blaaderen, A. Direct Observation of Dynamical Heterogeneities in Colloidal Hard-Sphere Suspensions. *Science* **2000**, *287*, 290−293.
(24) Woodcock, L. V. Developments in the Non-Newtonian Rheology of Glass Forming Systems. *Molecular Dynamics and Relaxation Phenomena in Glasses*; Springer Berlin Heidelberg: Berlin, Heidelberg, 2008; pp 113−124.
(25) Kamiya, H.; Otani, Y.; Fuji, M.; Miyahara, M. Characteristics and Behavior of Nanoparticles and Its Dispersion Systems. *Nanoparticle Technology Handbook*; Elsevier, 2018; pp 109−168.
(26) Guth, E. Theory of Filler Reinforcement. *J. Appl. Phys.* **1945**, *16*, 20−25.
(27) Donnet, J.-B.; Custodero, E. Reinforcement of Elastomers by Particulate Fillers. *The Science and Technology of Rubber*; Elsevier, 2013; pp 383−416.
(28) Fukahori, Y.; Hon, A. A.; Jha, V.; Busfield, J. J. C. Modified Guth-gold Equation for Carbon Black-filled Rubbers. *Rubber Chem. Technol.* **2013**, *86*, 218−232.
(29) Riggleman, R. A.; Toepperwein, G.; Papakonstantopoulos, G. J.; Barrat, J.-L.; de Pablo, J. J. Entanglement Network in Nanoparticle Reinforced Polymers. *J. Chem. Phys.* **2009**, *130*, 244903.
(30) Schneider, G. J.; Nusser, K.; Willner, L.; Falus, P.; Richter, D. Dynamics of Entangled Chains in Polymer Nanocomposites. *Macromolecules* **2011**, *44*, 5857−5860.
(31) Li, Y.; Kröger, M.; Liu, W. K. Nanoparticle Effect on the Dynamics of Polymer Chains and Their Entanglement Network. *Phys. Rev. Lett.* **2012**, *109*, 118001.
(32) Storm, C.; Pastore, J. J.; MacKintosh, F. C.; Lubensky, T. C.; Janmey, P. A. Nonlinear Elasticity in Biological Gels. *Nature* **2005**, *435*, 191−194.
(33) Sheiko, S. S.; Dobrynin, A. V. Architectural Code for Rubber Elasticity: From Supersoft to Superfirm Materials. *Macromolecules* **2019**, *52*, 7531−7546.
(34) Roland, C. M. Rheological Behavior and Processing of Unvulcanized Rubber. *The Science and Technology of Rubber*; Elsevier Inc., 2013; pp 285−336.
(35) Clair, C.; Lallam, A.; Rosenthal, M.; Sztucki, M.; Vatankhah-Varnosfaderani, M.; Keith, A. N.; Cong, Y.; Liang, H.; Dobrynin, A. V.; Sheiko, S. S.; Ivanov, D. A. Strained Bottlebrushes in Super-Soft Physical Networks. *ACS Macro Lett.* **2019**, *8*, 530−534.
(36) Keith, A. N.; Vatankhah-Varnosfaderani, M.; Clair, C.; Fahimipour, F.; Dashtimoghadam, E.; Lallam, A.; Sztucki, M.; Ivanov, D. A.; Liang, H.; Dobrynin, A. V.; Sheiko, S. S. Bottlebrush Bridge between Soft Gels and Firm Tissues. *ACS Cent. Sci.* **2020**, *6*, 413−419.

https://dx.doi.org/10.1021/acsami.0c11416
ACS Appl. Mater. Interfaces 2020, 12, 46621−46628